K-shell ionization of O^{4+} and C^{2+} ions in fast collisions with H_2 and He gas targets

D. H. Lee,* T. J. M. Zouros,† J. M. Sanders, and P. Richard
J.R. Macdonald Laboratory, Department of Physics, Kansas State University, Manhattan, Kansas 66506

J. M. Anthony
Department of Physics, U.S. Naval Academy, Annapolis, Maryland 21402

Y. D. Wang and J. H. McGuire
Department of Physics, Tulane University, New Orleans, Louisiana 70118
(Received 10 February 1992)

Cross sections for $1s$ ionization of the $1s^2 2s^2$ and $1s^2 2s2p\,^3P$ (metastable) states of C^{2+} and O^{4+} ions in 0.5–1.8 MeV/u collisions with H_2 and He targets were measured using projectile Auger electron spectroscopy at 0°. Calculations of the K-shell ionization cross section σ_K were performed including contributions from projectile-electron – target-nucleus interactions (σ_{enI}) within a plane-wave Born approximation (PWBA), and contributions from projectile-electron – target-electron interactions (σ_{eeI}) within an impulse approximation (IA). The theoretical total cross section $\sigma_K = \sigma_{enI} + \sigma_{eeI}$ was found to be in overall agreement with the K-shell ionization measurements indicating a contribution of up to $\sim 30\%$ due to electron-electron interactions. Separate screening-antiscreening calculations of σ_K were also performed and found to be in overall agreement with our data. Additionally, our PWBA-IA ionization calculation was also tested for H-like projectiles and found to be in agreement with recently published data. These results suggest that the IA calculation of σ_{eeI} when combined with a PWBA calculation of σ_{enI} is quite adequate for describing K-shell ionization.

PACS number(s): 34.50.Fa, 34.80.Kw, 34.80.Dp, 35.80.+s

I. INTRODUCTION

In ion-atom collisions, basic processes such as excitation and ionization can be strongly influenced by the electronic structure of the collision partners [1]. While these processes have been traditionally attributed to the Coulomb interaction between the promoted electron and the exciting nucleus (e-n interaction) [2], the "spectator" electrons can also individually interact with the promoted electron (e-e interaction), either in a static role by screening the Coulomb field of the exciting nucleus or in a dynamic role by directly participating in the collision process [2]. An accurate account of excitation or ionization must therefore correctly include contributions from both e-n and e-e interactions. While several authors have previously considered the influence of e-e contributions to total target [3] and projectile [4–6] ionization, it is only quite recently that unambiguous signatures of e-e interactions in excitation and ionization have been demonstrated [7, 8].

Such recent investigations in fast collisions of highly charged ion projectiles with H_2 and He targets have shown that the dynamic role of spectator electrons can account for up to 60% of the cross section for $1s$ projectile ionization at high collision energies [8–10] or can exhibit distinct threshold effects in the projectile energy dependence of the measured cross sections for $1s \rightarrow 2p$ projectile excitation [7, 11, 12]. The static role of spectator electrons has also recently been observed in the "anomalous" screening of the projectile nuclear charge by projectile electrons in the case of binary-encounter-electron [13–22] and δ-electron production [15, 16, 23]. These recent developments have shown that studies of such e-e effects are both experimentally feasible and can contribute new insights to our understanding of basic ion-atom collision processes. Sections I A and I B present the screening-antiscreening and impulse-approximation (IA) approaches used in the study of ion-atom collisions and applied to the analysis of K-shell projectile ionization.

A. Screening-antiscreening approach

Early theoretical investigations of ionization focused on inner-shell-vacancy production in atoms by fast *bare* projectiles. Much effort went into the plane-wave Born approximation (PWBA) treatment of excitation and ionization in fast ion-atom collisions (see, for example, Refs. [24–29]). The PWBA is valid when $Z << V_0 \lesssim v$ (in a.u.) [24] where V_0 is the collision velocity. We shall use the convention that the exciting-agent parameters are given in uppercase letters, while the promoted-electron parameters are given in lowercase letters, since the same formulation can be used either for ionization of the target by the projectile or of the projectile by the target. Thus, for *target* ionization, v is the orbital velocity of the target electron to be ionized, while Z refers to the projectile nuclear charge. For *projectile* ionization, v is the orbital

velocity of the projectile electron to be ionized and Z refers to the target nuclear charge. In Fig. 1, a schematic diagram of a one-electron projectile colliding with a target atom (as seen from the projectile rest frame) shows the relevant parameters involved in the problem of projectile excitation and ionization. The PWBA approach has been quite successful in the calculation of ionization cross sections of atoms by bare projectiles, a well-known result being that the target Coulomb ionization cross sections scale with Z^2 [26, 30].

Bates and Griffing [31] did pioneering work in the theoretical study of excitation and ionization in H + H collisions; however, systematic studies of the dependence of target ionization cross sections on the number of electrons carried into the collision by the projectile appeared much later [32–36, 1, 37]. Investigations focused primarily on the quantitative description of the screening effects of the projectile nuclear charge Z by the projectile electrons. Typical experiments measured ionization cross sections of many-electron target atoms and their dependence on the projectile charge state, as for example in 30-MeV $O^{(4-8)+}$ on O_2 [33] or 0.3–1.2-MeV $He^{(1-2)+}$ on Ar [34].

Within the PWBA, the total target ionization cross section can be expressed in terms of the product of two quantities, $|f(q)|^2$ (in a.u.) and $[Z^*(q)]^2$, dependent on the momentum transfer q. The form factor $f(q)$ depends only on target properties, while the effective charge of the projectile $Z^*(q)$ is entirely independent of the target [1]. Thus, the effect of the projectile electrons is to either decrease or increase the cross sections relative to those for a bare projectile, by scaling the bare projectile results by Z^{*2}. Specifically, for a projectile of nuclear charge Z carrying N electrons into the collision, in the limit of small q (corresponding to large impact parameters), $[Z^*(q)]^2$ approaches $(Z-N)^2$ corresponding to the total screening of the projectile. In the limit of large q (corresponding to small impact parameters), $[Z^*(q)]^2$ goes to Z^2+N corresponding to incoherent scattering by the projectile nucleus and N electrons. This leads to an effective enhancement of the cross sections that has been named antiscreening. The variation of Z^* with q is known as "screening-antiscreening" [1, 32]. From these limiting cases, it is clear that the effect of the electrons is strongest for low-Z values. Various formulas for the effective projectile charge Z^* were found to be in fair agreement with the available experimental data [1, 37], while reported discrepancies were blamed on electron capture, which was not included in the ionization calculations. Capture can also lead to vacancy production in the target atom, thus complicating the interpretation of the data. This difficulty was overcome in later experiments by studying the ionization of the projectile ion rather than that of the neutral target.

Even though it had been recognized that the electron can sometimes act passively as a "spectator," just screening the nuclear Coulomb field, while at other times it can act dynamically to increase the ionization cross section, constraints due to conservation of energy on the electron contributions were initially neglected [4]. This omission was corrected in the work of Anholt *et al.* [4, 38] concerning projectile ionization where it was recognized that the e-e excitation contributions should be reduced at low velocities, because the target electrons do not have sufficient kinetic energy (in the projectile frame) to excite the projectile electron. Thus, a correction of the PWBA approach to screening-antiscreening was included to account for this omission [38]. Then the cross section for $1s$ ionization of one of the structured particles by the other (following the aforesaid convention) is given within the closure approximation (in a.u.) by [1, 8]

$$\sigma_K = (8\pi/V_0^2)\int_0^\infty d\varepsilon \int_{q_0}^\infty (dq/q^3)|f(q)|^2|Z^*(q)|^2, \qquad (1)$$

where q_0 is the minimum momentum transfer [38], ε is the kinetic energy of the ionized electron, and Z^* is the nuclear charge of the ionizing agent. Applying this to the case of projectile ionization, $f(q) = \langle \varepsilon | e^{i\mathbf{q}\cdot\mathbf{r}} | 1s \rangle$ is the form factor of the projectile electron, while the effective charge of the target is given by

$$|Z^*(q)|^2 = [Z - |F(q)|]^2 + \left[Z - \sum_j^Z |F_j(q)|^2\right]\sigma_{eII}(V_0)/\sigma_p(V_0), \qquad (2)$$

where $F_j = \langle j | e^{i\mathbf{q}\cdot\mathbf{r}} | j \rangle$ is the form factor for the jth target electron, Z is the target nuclear charge, and $F = \sum_j F_j$. The electron-impact-ionization (eII) cross section $\sigma_{eII}(V_0)$ is for an electron of velocity equal to the projectile velocity V_0. For impact energies smaller than the ionization threshold, $\sigma_{eII}(V_0)$ is zero. $\sigma_p(V_0)$ is the PWBA ionization cross section of the projectile ion by a proton of velocity V_0. The upper limit for the mo-

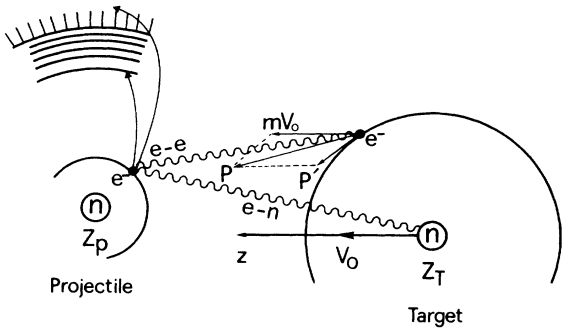

FIG. 1. Schematic diagram of an ion-atom collision showing the different interactions between nuclei and electrons. For simplicity only one electron is shown on each projectile (P) and target (T). The projectile electron is shown to be excited or ionized by interacting with the target nucleus (e-n interaction) or target electron (e-e interaction). The target electron has a net momentum $\mathbf{P} = \mathbf{P}_0 + \mathbf{P}'$ in the projectile frame, where $\mathbf{P}_0 = m\mathbf{V}_0$ and $\mathbf{P}' = m\mathbf{V}'$ is its orbital momentum due to its motion around the target. $\mathbf{V}_0$ is the ion-atom collision velocity and m is the electron mass.

mentum transfer in eII is taken to be $q = \infty$, so that the ratio $\sigma_{eII}/\sigma_p = 1$ at very high q. This formula then gives the expected limiting cases of $Z^{*2} = Z^2 + N$ and $Z^{*2} = (Z - N)^2$ for very-high- and very-low-momentum transfer, respectively. In the case of a neutral target, $N = Z$. The two terms in Eq. (2) can be interpreted physically in terms of ionization by the exciting agent's screened nuclear charge (screening), and its electrons (antiscreening), respectively [9].

Using this screening-antiscreening PWBA calculation, the first evidence of an e-e interaction in inner-shell ionization was elucidated from projectile K-shell ionization experiments using low-Z targets [8]. In that study [8], projectile K-shell ionization cross sections were measured for 0.75–3.5 MeV/u C^{5+} and O^{7+} projectiles in collisions with H_2 and He targets. The projectile charge state following ionization was identified by electrostatic analysis, and the number of ionized projectiles were counted to determine the total $1s$ ionization cross section as a function of the collision energy. For collision energies above the threshold for electron-impact ionization, the measured cross sections were found to be as much as two times larger than the expected PWBA results for pure e-n ionization, as seen in the results for $C^{5+} + H_2$ shown in Fig. 2. The screening-antiscreening calculations agree well with the data, which indicates the existence of ionization due to e-e interactions [8–10]. Also shown in Fig. 2 are the results of our PWBA-IA treatment discussed next.

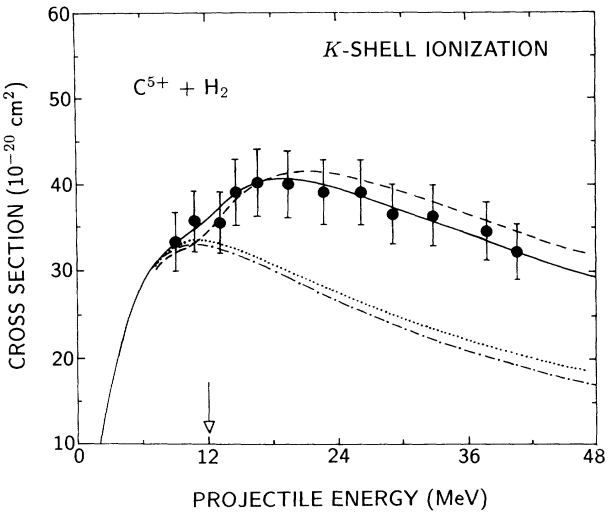

FIG. 2. Data: K-shell projectile-ionization cross section σ_K for $C^{5+}(1s)$ collisions with H_2 targets obtained by the charge-analysis method of Ref. [8]. Solid line: PWBA-IA calculation of $\sigma_K = \sigma_{enI} + \sigma_{eeI}$ (this work, see Sec. IV). Dashed line: PWBA screening-antiscreening calculations of σ_K using Eq. (1) (from Ref. [8]). Dashed-dotted line: scaled PWBA calculation of σ_{enI} given by Eq. (19). Dotted line: PWBA calculation of σ_K (screening part only) considering only an e-n interaction (from Ref. [8]). The arrow indicates the projectile energy corresponding to the $1s$ ionization threshold for the electron impact of the same velocity.

B. Impulse-approximation approach

A different approach to electron-electron interactions based on the impulse approximation (IA) [39], has enjoyed a parallel development [40–42], particularly in its successful application [42] to the understanding of resonance transfer and excitation (RTE) [43]. RTE has received considerable attention, since it can provide direct information on electron-electron interaction phenomena [44] presently of great interest in atomic physics.

The IA method, generally used in nuclear physics scattering problems during the early 1940s and 1950s [45], was first investigated in detail [39] for studies of Compton scattering of x rays off lightly bound electrons. The IA was later successfully applied to the description of radiative electron capture [40] and RTE [42]. The basic assumption of the IA is that when the collision time τ_c is short compared to the orbiting time of the bound electron acting as the excitation agent, this electron can be considered to interact as a free particle, since its potential does not change appreciably over the time τ_c. Thus, the three-body problem involving the incoming projectile, the target electron, and the target nucleus is converted to a simpler two-body problem involving only the projectile and target electron.

The IA has been successfully used to describe a variety of other ion-atom collision processes involving "quasi-free" target electrons, including projectile electron-electron excitation (eeE) [7, 11, 12], RTE [46–50] and binary encounter electron production [30, 13]. In this paper we extend the impulse approximation to the problem of projectile electron-electron ionization (eeI) in ion-atom collisions.

The mathematical formulation of the IA is straightforward. As viewed from the projectile frame, the target electron approaches the projectile ion with kinetic energy E_e, broadened by its momentum distribution due to its orbital motion around the target nucleus; it interacts with the ion as a free particle with an electron-impact cross section $\sigma_{eI}(E_e)$. The effective electron-electron interaction cross section in the ion-atom collision σ_{ee} is obtained by summing over the contributions of all target electrons i which is given within the IA by [40, 42, 30]

$$\sigma_{ee}(E_p) = \sum_i \int d^3\mathbf{P}_i \sigma_{eI}(E_{e_i}) |\Psi_i(\mathbf{P}_i - \mathbf{P}_0)|^2. \quad (3)$$

The ith target electron will have an effective momentum $\mathbf{P}_i$ in the projectile frame, with an initial momentum distribution described by $|\Psi_i(\mathbf{P}_i - \mathbf{P}_0)|^2$ which is peaked around $\mathbf{P}_0 = m\mathbf{V}_0$, since the electron is moving with this average momentum in the projectile frame [40]. Ψ_i is the *momentum* wave function of the ith interacting target electron. The energy of the projectile ion is given by $E_p = \frac{1}{2} M_p V_0^2$, where M_p is the mass of the ion.

For a target electron in the $1s$ orbital with ionization energy I_{1s} and orbital momentum $\mathbf{P}' = \mathbf{P} - \mathbf{P}_0$, its kinetic energy E_e can be written from energy conservation considerations as [42, 30]

$$E_e = \frac{P^2}{2m} - I_{1s} \tag{4}$$

$$= \frac{m}{M_p}E_p + V_0 P'_z + \frac{P'^2}{2m} - I_{1s}, \tag{5}$$

where the z axis has been chosen to lie along $\mathbf{V}_0$. The terms I_{1s} and $P'^2/2m = (P'^2_x + P'^2_y + P'^2_z)/2m$, for fast enough collisions, are negligible compared to $mE_p/M_p = P_0^2/2M_p$ [42]. However, the terms I_{1s} and P'^2_z are retained here, as this has been shown to give improved agreement with experimental results [30, 51] without complicating the calculation. Thus, we finally obtain

$$E_e = \frac{m}{M_p}E_p + V_0 P'_z + \frac{P'^2_z}{2m} - I_{1s}. \tag{6}$$

Using the definition of the Compton profile [40] for the ith electron

$$J_i(P'_{z_i}) = \int dP'_{x_i} dP'_{y_i} |\Psi_i(\mathbf{P}'_i)|^2, \tag{7}$$

Eq. (3) can be written in the simpler form

$$\sigma_{ee}(E_p) = \sum_i \int \sigma_{eI}[E_e(P'_{z_i})] J_i(P'_{z_i}) dP'_{z_i}, \tag{8}$$

which can be readily integrated over P'_{z_i} for known Compton profiles $J_i(P'_{z_i})$ [52]. Thus, the impulse approximation is seen to directly relate phenomena of electron-electron interactions in ion-*atom* collisions to electron-impact phenomena in ion-*electron* collisions. Furthermore, this relation can work in both directions so that knowledge of either σ_{eI} or σ_{ee}, through Eq. (8), can give information about the other. In the case of projectile electron-electron ionization of interest here, σ_{ee} will be the ion-atom ionization cross section σ_{eeI} and σ_{eI} will be the corresponding electron-impact ionization cross section σ_{eII}. The calculation of σ_{eeI} by Eq. (8) is presented in detail in Sec. IV.

Following this introduction, in Sec. II the experimental part of the study is described, while in Sec. III the analysis of the data is presented. In Sec. IV we present the theoretical calculations within the IA approach to account for e-e interactions, and in Sec. V we discuss various problems of this analysis and compare our measured ionization cross sections with the results of a screening-antiscreening calculation.

II. EXPERIMENT

The measurements were performed at the J.R. Macdonald Laboratory at Kansas State University using the 7.5-MV tandem Van de Graaff accelerator. Be-like O^{4+} and C^{2+} beams were accelerated to energies between about 0.5 and 1.8 MeV/u and collided with H_2 or He gas targets. When the projectile ion was initially in the ground-state $1s^2 2s^2\ ^1S$ configuration, the loss of a $1s$ projectile electron left the ion in the $1s2s^2\ ^2S$ state. The Auger electron emitted from the filling of the $1s$ vacancy through autoionization was detected at 0° with respect to the beam direction using high-resolution projectile Auger spectroscopy [53, 54]. Schematically, if T represents the target (He or H_2) and P the projectile, for $1s$ ionization followed by Auger relaxation we have

$$P^{q+}(1s^2 2s^2) + T(1s^2)$$

$$\longrightarrow P^{q+1}(\,1s2s^2\ ^2S) + T(?) + e^- \quad (1s \text{ ionization})$$

$$\hookrightarrow P^{q+2}(1s^2) + e^- \quad (\text{Auger decay}).$$

A large fraction of the beam (about 61%, see Sec. III) was found to be in the metastable $1s^2 2s2p\ ^3P$ state [55]. The metastable ion, upon losing a $1s$ electron, also decayed through autoionization giving rise to three distinct lines in the electron spectra [56]

$$P^{q+}(1s^2 2s2p\ ^3P) + T(1s^2) \longrightarrow \begin{cases} P^{q+1}[1s2s2p\ ^4P] \\ P^{q+1}[1s(2s2p\ ^3P)\ ^2P_-] \\ \underbrace{P^{q+1}[1s(2s2p\ ^1P)\ ^2P_+]} \end{cases} + T(?) + e^- \quad (1s \text{ ionization})$$

$$\hookrightarrow P^{q+2}(1s^2) + e^- \qquad (\text{Auger decay})$$

The final state of the target was not determined in these measurements.

The experimental apparatus and analysis procedures for 0° electron spectroscopy used at Kansas State have been previously described in detail [7, 57] and therefore are not presented here. The absolute efficiency for electron detection was determined by normalizing to the binary encounter peak [58] produced by bare ions in collisions with H_2 using the IA [30]. This has been found to be a direct and accurate [59–62] way of obtaining *in situ* absolute efficiencies for our electron detection apparatus [60].

III. DATA ANALYSIS

A. Double-differential electron yields and Auger line identification

The double-differential cross section for Auger electron production is

$$\frac{d^2\sigma}{dEd\Omega} = \frac{N_e}{Nnl\Delta E\Delta\Omega\eta}, \tag{9}$$

where N_e is the detected electron count at a given Auger electron energy E and a given detection angle ($\theta = 0°$ in our work), n and l are the target gas density and the gas cell length, ΔE is the spectrometer acceptance energy at electron energy E, and $\Delta\Omega$ and η are the effective solid angle and efficiency of the electron spectrometer. N is the number of projectiles in either the ground or metastable state.

Double-differential electron yields were obtained from

$$\frac{d^2Y}{dEd\Omega} = \frac{N_e}{N_0nl\Delta E\Delta\Omega\eta}, \tag{10}$$

where

$$N_0 = N_g + N_m \tag{11}$$

is the total number of incoming projectiles. These projectiles were collected in a Faraday cup and therefore consisted of ions in both the ground (N_g) and metastable (N_m) states. In Figs. 3 and 4 electron yields evaluated by Eq. (10) are shown for 10–28.5-MeV O^{4+} collisions with H_2 and He targets and for 5–18-MeV C^{2+} collisions with H_2 targets. The normalized double-differential electron yields at $\theta = 0°$ are displayed after the subtraction of background continuum electrons and transformation to the projectile frame.

The various KLL Auger lines observed in the spectra were identified with the help of previous spectroscopic studies and theoretical calculations [56,63–74]. The energies of the Auger lines are summarized in Tables I and II. The lines were fitted by Lorentzian functions folded with the response function of the electron spectrometer, and from these fits single-differential electron yields $dY/d\Omega$ could be obtained. As can be seen from Figs. 3 and 4 the $1s2s^2\,{}^2S$ line and the $1s2s2p\,{}^4P$ line are quite strong and clearly resolved. The other two ionization lines, ${}^2P_+$ and ${}^2P_-$, are weaker and less clearly resolved. All other lines in the spectra are due to the decay of Be-like configurations produced by excitation. The processes that can give rise to the various lines in the spectra are summarized in the schematic diagram shown in Fig. 5.

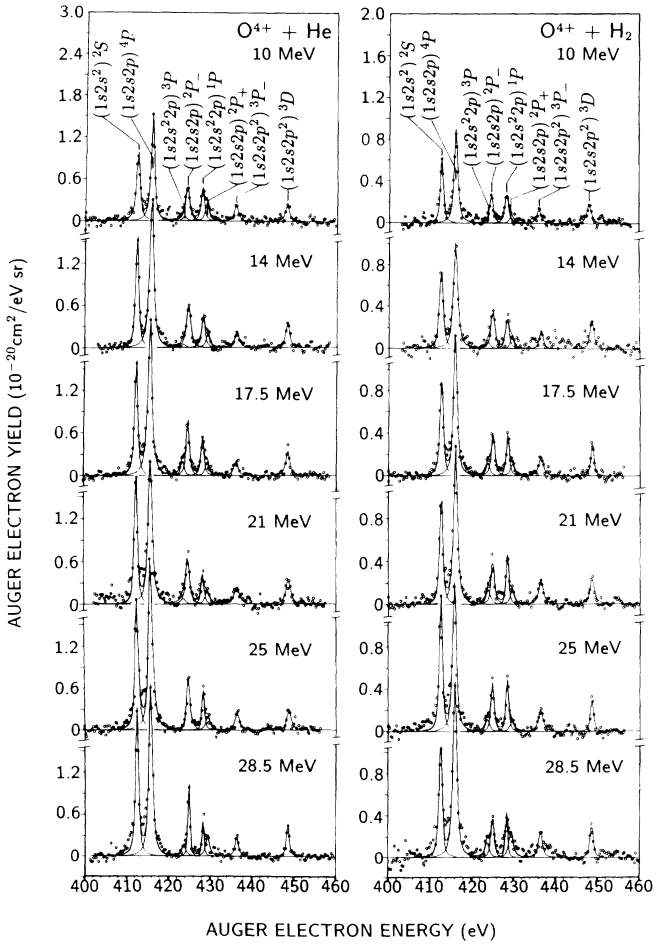

FIG. 3. Normalized 0° Auger electron spectra measured for 10–28.5-MeV O^{4+} collisions with H_2 and He targets after subtraction of background continuum electrons and transformation to the projectile frame. The $1s2s^2\,{}^2S$ line results from $1s$ ionization of the ground state. The ${}^4P$, ${}^2P_-$ and ${}^2P_+$ states result from $1s$ ionization of the metastable $1s2s2p^2\,{}^3P$ ion. All other lines are due to the decay of Be-like configurations produced by excitation.

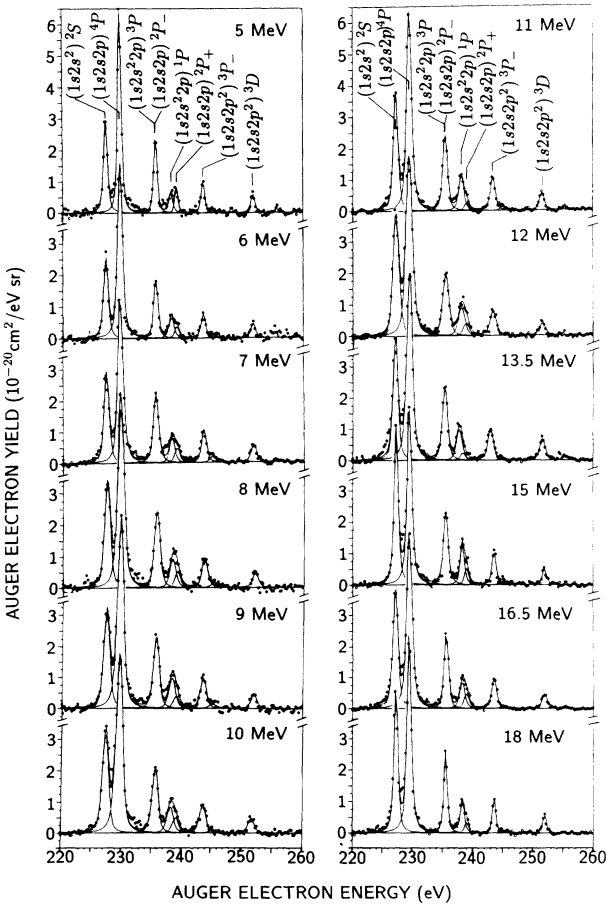

FIG. 4. Same as Fig. 3, but for 5–18-MeV C^{2+} collisions with H_2 targets.

TABLE I. Theoretical (E_{theor}) and experimental (E_{expt}) Auger line energies and their difference (in eV) for O^{4+} collisions with H_2 and He targets. The initial states of the ion are the $1s^2 2s^2\ ^1S$ and $1s^2 2s2p\ ^3P$ metastable states (see Fig. 5). The intermediate states are produced in the collision by 1s ionization or excitation, which then decay by Auger electron emission to the final state. The Auger yield ξ of this transition is also listed.

Initial state	Intermediate state	Final state	E_{theor} (eV)[a]	E_{expt} (eV)[b]	Diff. (eV)	ξ
$1s^2 2s^2\ ^1S$	$1s2s^2\ ^2S$	$1s^2$	412.6	412.7	−0.1	1.000[c]
$1s^2 2s2p\ ^3P$	$1s2s2p\ ^4P$	$1s^2$	416.0	416.0	0.0	0.895[d]
$1s^2 2s^2\ ^1S$	$1s2s^2 2p\ ^3P$	$1s^2 2p$	424.2	423.7	0.5	
$1s^2 2s2p\ ^3P$	$1s2s2p\ ^2P_-$	$1s^2$	425.0	424.9	0.1	0.739[e]
$1s^2 2s^2\ ^1S$	$1s2s^2 2p\ ^1P$	$1s^2 2p$	428.5	428.4	0.1	
$1s^2 2s2p\ ^3P$	$1s2s2p\ ^2P_+$	$1s^2$	429.7	429.5	0.2	0.996[e]
$1s^2 2s2p\ ^3P$	$1s2s2p^2\ ^3P_-$	$1s^2 2p$	436.4	436.4	0.0	
$1s^2 2s2p\ ^3P$	$1s2s2p^2\ ^3D$	$1s^2 2s$	448.0	448.2	−0.2	0.899[f]

[a]Reference [56].

[b]This work. Experimental errors are about ±0.2 eV. For the electron-energy calibration, the ^4P Auger line was used as the reference standard. The measured energies are in good agreement with those previously measured in Ref. [56].

[c]Reference [63].

[d]Mean Auger yield $\xi = \sum_J a_J \xi_J$, where a_J is the statistical weight of the J substates, i.e, $a_J = (2J+1)/\sum_J (2J+1)$. ξ_J is given in Refs. [64] and [65].

[e]Reference [66].

[f]Reference [46].

B. K-shell ionization cross section and the $1s^2 2s2p\ ^3P$ metastable beam fraction

The K-shell ionization cross section σ_K^g of the ground-state ion can be directly determined from the measured Auger electron yield of the $1s2s^2\ ^2S$ state using Eqs. (9), (10), and (11). We thus obtain

$$\sigma_K^g = \frac{1}{\xi_{2S}} \int\int \frac{d^2Y_{2S}}{dE\,d\Omega} \frac{N_0}{N_g} dE\,d\Omega \equiv \frac{Z_{2S}}{F_g}, \tag{12}$$

where ξ_{2S} is the Auger yield (see Table I), and $F_g = N_g/N_0$ is the ground-state beam fraction. We define Z_{2S} to be the state-production yield determined from the electron yield of the $1s2s^2\ ^2S \rightarrow 1s^2\ ^1S$ Auger transition

$$Z_{2S} \equiv \frac{1}{\xi_{2S}} \int\int \frac{d^2Y_{2S}}{dE\,d\Omega} dE\,d\Omega. \tag{13}$$

In the case of 1s ionization of the metastable ion, we must include all the Auger electrons from the three states

TABLE II. Same as Table I but for C^{2+} + H_2 collisions. Energies are given in eV.

Initital state	Intermediate state	Final state	E_{theor}[a]	E_{theor}[b]	E_{theor}[c]	E_{theor}	E_{expt}[a]	E_{expt}[c]	E_{expt}[d]	E_{expt}[e]
$1s^2 2s^2\ ^1S$	$1s2s^2\ ^2S$	$1s^2$	227.2	227.2	227.5		227.1	227.5	227.6	227.4
$1s^2 2s2p\ ^3P$	$1s2s2p\ ^4P$	$1s^2$	229.8	229.6		229.7[f]	229.6	229.9	229.7	229.7
$1s^2 2s^2\ ^1S$	$1s2s^2 2p\ ^3P$	$1s^2 2p$	235.3	235.4	235.9	235.2[g]	235.1	235.5	235.5	235.7
$1s^2 2s2p\ ^3P$	$1s2s2p\ ^2P_-$	$1s^2$	235.3	235.5	235.9	235.8[h]	235.5			235.7
$1s^2 2s^2\ ^1S$	$1s2s^2 2p\ ^1P$	$1s^2 2p$			238.5				238.3	238.3
$1s^2 2s2p\ ^3P$	$1s2s2p\ ^2P_+$	$1s^2$	239.4	238.8	239.3		238.9	238.9	239.0	239.1
$1s^2 2s2p\ ^3P$	$1s2s2p^2\ ^3P_-$	$1s^2 2p$	241.7			243.4[h]				243.6
$1s^2 2s2p\ ^3P$	$1s2s2p^2\ ^3D$	$1s^2 2s$				252.3[i]				251.9

[a]Reference [67].

[b]Reference [68].

[c]Reference [69].

[d]Reference [70].

[e]This work. Experimental errors are about ±0.15 eV. For the electron-energy calibration, the ^4P Auger line was used as the reference standard.

[f]Reference [71].

[g]Reference [74]

[h]Reference [72].

[i]Reference [73].

(see Fig. 5) which are formed by $1s$ ionization of the $1s^2 2s 2p\,{}^3P$ metastable state

$$\sigma_K^m = \sum_L \frac{1}{\xi_L} \int\int \frac{d^2Y_L}{dE\,d\Omega} \frac{N_0}{N_m} dE\,d\Omega$$
$$= \frac{Z_{^4P}}{F_m} + \frac{Z_{^2P_-}}{F_m} + \frac{Z_{^2P_+}}{F_m}, \tag{14}$$

where Z_L is defined for the three states, ${}^4P$, ${}^2P_-$, and ${}^2P_+$, analogously to $Z_{^2S}$ in Eq. (13).

In order to complete the integrations over the solid angle $d\Omega$ in Eqs. (13) and (14) and extract a total ionization cross section from the Auger electron yields $dY/d\Omega$ at $\theta = 0°$, isotropic emission of Auger electrons was assumed for all the Auger ionization lines. We note that the determination of $Z_{^4P}$ must also include the appropriate corrections [51, 12] due to the long lifetime of this state [64, 65, 75, 76] which affects the effective detection solid angle [77].

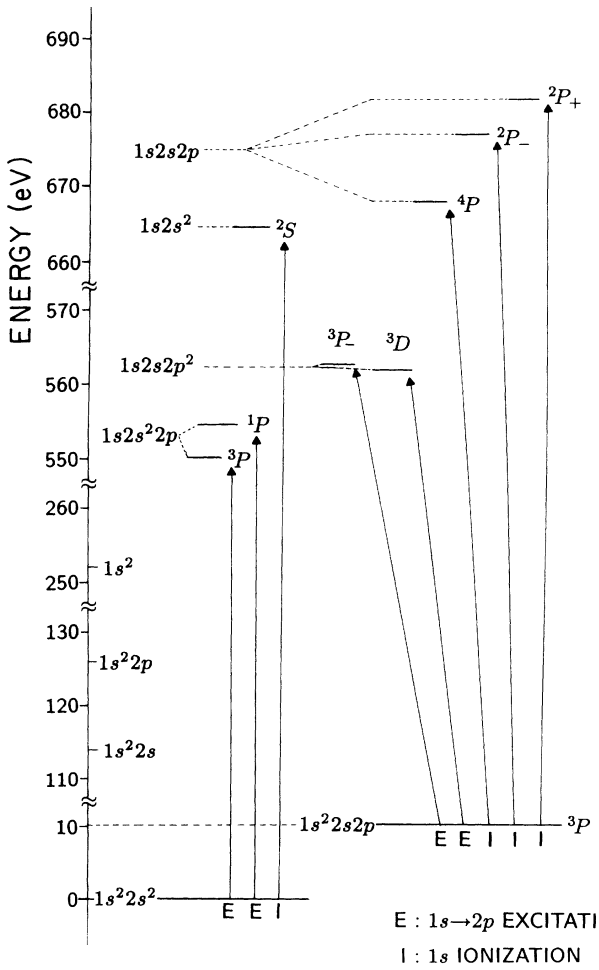

FIG. 5. Schematic energy-level diagram showing how excitation or ionization of the ground state $O^{4+}(1s^2 2s^2\,{}^2S)$ or the metastable state $O^{4+}(1s^2 2s 2p\,{}^3P)$ can lead to the production of the intermediate states observed in the spectra of Figs. 3 and 4. The same processes occur in C^{2+} collisions.

To evaluate the $1s$ ionization cross sections, the ground state and metastable beam fractions F_g and F_m must be known. These fractions can be obtained directly from the extracted single-electron yields of the ionization (Li-like) lines in the spectra [54] (see Figs. 3 and 4). This analysis is presented next.

The basic premise underlying the determination of F_m is that the cross section for the $1s$ ionization of the ground state is the same as that for the metastable state. This premise, experimentally verified in high-resolution K x-ray studies, has been used before in the determination of the metastable beam fraction of He-like ions [61]. It is well known [61, 53, 78, 79] that light targets such as H_2 or He have the ability to ionize selectively a single $1s$ projectile electron without disturbing the outer-shell electrons, a situation referred to as "needle" ionization [53, 78, 79]. Needle-ionization conditions prevail at fast collision velocities, as discussed in detail in Refs. [56] and [79] concerning fast O^{4+} collisions with light targets. Therefore, under needle-ionization conditions, the ionization of the K-shell is assumed to be unaffected by differences in the outer-shell configurations, and we set $\sigma_K^g = \sigma_K^m$. Setting Eq. (12) equal to Eq. (14) and using $F_g + F_m = 1$ we obtain

$$F_m = \left[1 + \frac{Z_{^2S}}{Z_{^4P} + Z_{^2P_-} + Z_{^2P_+}}\right]^{-1}. \tag{15}$$

Using Eq. (15) and the measured Auger yields, F_m can in principle be determined; in practice, however, corrections to the ${}^4P$ electron yield due to its long lifetime makes Eq. (15) difficult to evaluate accurately. To avoid this problem, a different method was developed for determining F_m, using only the electron yields from the prompt ${}^2S$ and ${}^2P_-$ lines. This method is described next.

Ionization of the $1s$ electrons of the ground-state ion can contribute only to the formation of the ${}^2S$ state. However, in the case of the $1s$ ionization of the metastable state the situation is somewhat complicated. Following the ionization of a $1s$ electron, the three remaining electrons recouple according to the rules for the addition of angular momenta forming the three states: ${}^4P$, ${}^2P_-$, and ${}^2P_+$. From tables of fractional parentage coefficients [80], the relative probabilities for the formation of these states can be found to be 4:3:1, respectively [81, 82].

Therefore, the production probabilities for the ${}^2S$, ${}^4P$, ${}^2P_-$, and ${}^2P_+$ states, under the assumption $\sigma_K^g = \sigma_K^m$, will be in the ratio of 8:4:3:1. Using these relations we obtain

$$\sigma_{^2S} = 2\sigma_{^4P} = \tfrac{8}{3}\sigma_{^2P_-} = 8\sigma_{^2P_+}, \tag{16}$$

where σ_L is the state-production cross section of the Auger line L, e.g., $\sigma_{^2S} = Z_{^2S}/F_g$ or $\sigma_{^2P_-} = Z_{^2P_-}/F_m$. Equation (16) provides another way of determining the metastable beam fraction F_m requiring only the measurement of the yields of the ${}^2S$ line and just one of the lines resulting from the ionization of the metastable beam component. The best Auger line for this purpose is the ${}^2P_-$ line which, for O^{4+}, is both resolved from the other lines (see Fig. 6) and does not require a lifetime correc-

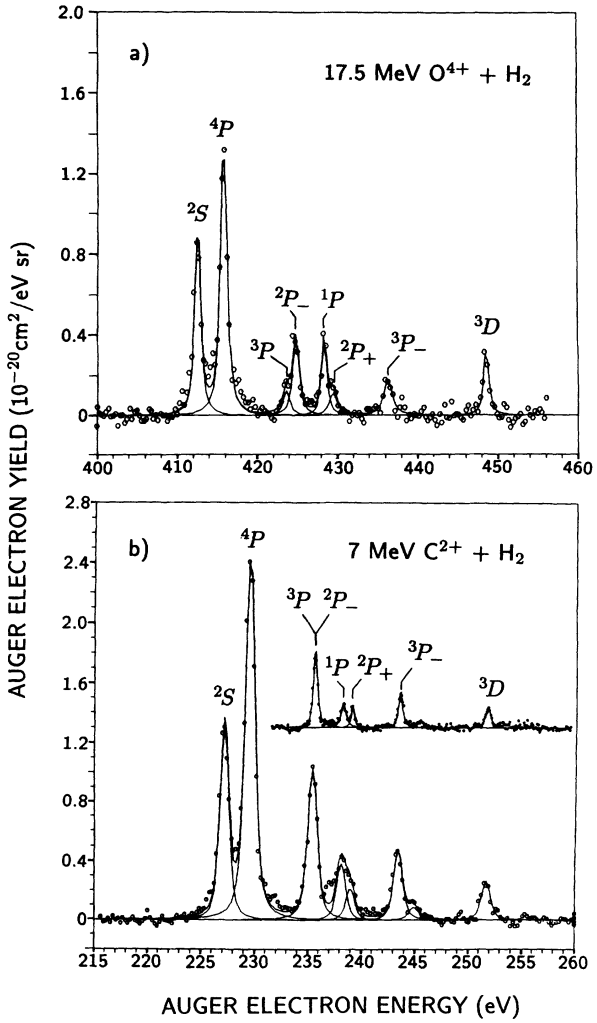

FIG. 6. Comparison between the O^{4+} and C^{2+} projectile Auger electron spectra. The ^3P and $^2P_-$ Auger lines (see Tables I and II) could not be resolved, in the case of C^{2+} projectile ions, even in the very-high-resolution spectrum shown (inset).

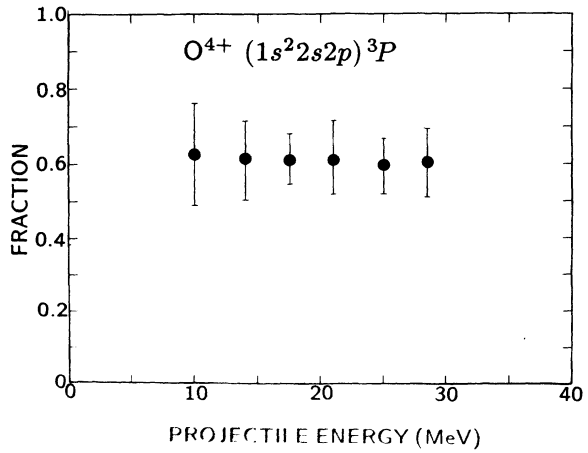

FIG. 7. Metastable beam fractions F_m for O^{4+} + He and H_2 collisions experimentally determined using Eq. (17) (see text).

tion like the long-lived ^4P line. Thus from Eqs. (15) and (16) we obtain

$$F_m = \left[1 + \frac{3}{8}\frac{Z_{2S}}{Z_{2P_-}}\right]^{-1}. \tag{17}$$

The experimentally determined fraction F_m, using Eq. (17), is shown in Fig. 7 for O^{4+} projectiles. Both He and H_2 targets gave very similar results and thus only the average for both targets is shown in Fig. 7. The fraction is fairly constant within the experimental error over the whole range of projectile energies. The average value for all projectile energies is found to be 0.61 ± 0.06. This is consistent with the reported value of 0.60 ± 0.05 measured for 10-MeV O^{4+} + He collisions [56]. Consistent results are also obtained when we use Eq. (15) with the correction factor for the detection efficiency of the long-lived

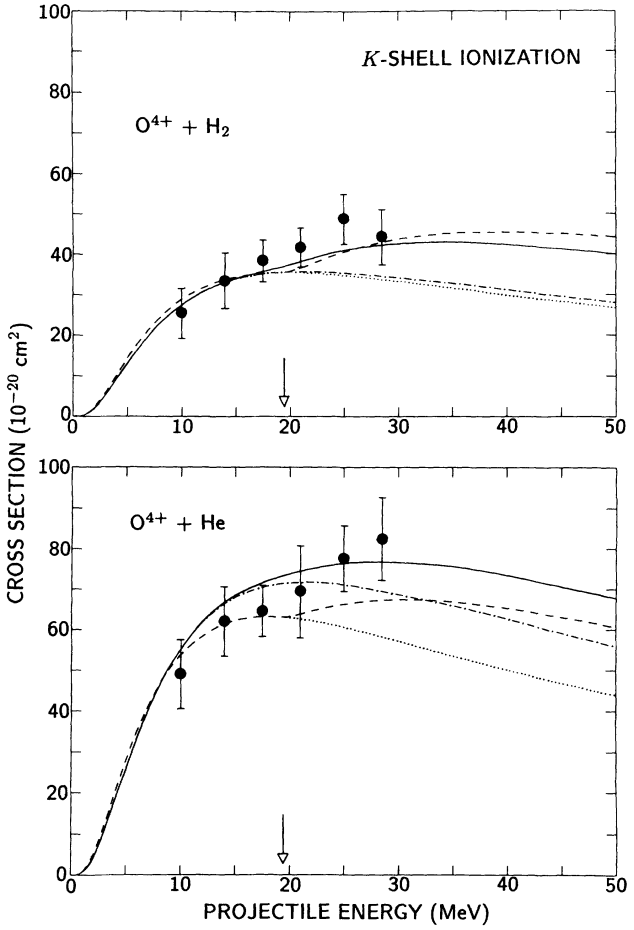

FIG. 8. K-shell projectile-ionization cross section σ_K for 10–28.5-MeV O^{4+} + H_2 and He collisions. Solid line: PWBA-IA calculation of $\sigma_K = \sigma_{enI} + \sigma_{eeI}$ (this work, see Sec. IV). Dashed line: PWBA screening-antiscreening calculations of σ_K (this work) using Eq. (1) [89]. Dashed-dotted line: scaled PWBA calculation of σ_{enI} given by Eq. (19). Dotted line: PWBA calculation of σ_K (screening part only) considering only an e-n interaction (this work) [89]. The arrow indicates the projectile energy corresponding to the $1s$ ionization threshold for the electron impact of the same velocity.

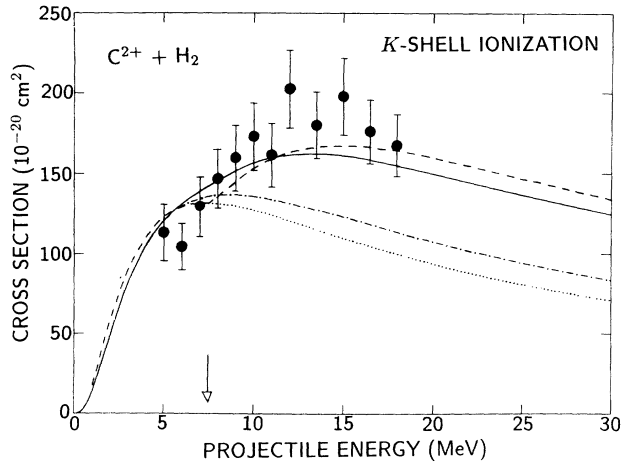

FIG. 9. Same as Fig. 8, but for 5–18-MeV C^{2+} collisions with H_2 targets.

^4P state. In this case, F_m was found to be 0.59 ± 0.04 [77].

The $^2P_-$ state is resolved in the case of O^{4+} projectiles as seen in Fig. 6 (top); however, it cannot be resolved in the case of C^{2+} projectiles from the close-lying $1s2s^22p\,^3P$ excitation line, even in the very-high-resolution spectrum ($\Delta E \sim 0.5$ eV), shown in the inset of Fig. 6 (bottom). This is consistent with the theoretical Auger energies as seen in Table II. Thus, in the case of C^{2+} projectiles, the $^2P_-$ state cannot be used in Eq. (17). Furthermore, the $^2P_+$ line is too weak to be used instead of the $^2P_-$ state. Therefore, for C^{2+}, the value of $F_m = 0.64 \pm 0.06$, determined in Ref. [82] was used in the data analysis for all C^{2+} projectile energies.

Following the determination of F_m, the K-shell ionization cross section σ_K was directly obtained utilizing Eqs. (12) and (13) and the ^2S Auger electron yield whose angular distribution is known from theory to be isotropic [83–85]. We thus obtain

$$\sigma_K = \frac{Z_{2S}}{F_g} = \frac{4\pi}{F_g \xi_{2S}} \frac{dY_{2S}}{d\Omega}(0°). \tag{18}$$

The extracted cross sections are plotted as a function of projectile energy in Figs. 8 and 9.

IV. PWBA-IA CALCULATIONS

A. Contributions from the electron-nucleus interaction

The e-n contribution to the $1s$ ionization was obtained by scaling the PWBA ionization cross sections of $H^+ + H$ collisions as follows [86]:

$$\sigma_{enI}(E_p) = 2N_A \frac{Z^2}{z^{*4}} \sigma_{pH}(V_0/z^*) \left[\frac{13.6 z^{*2}}{i_{1s}}\right]^2 = 2N_A Z^2 \sigma_{pH}(V_0/z^*) \left[\frac{13.6}{i_{1s}}\right]^2. \tag{19}$$

Z is the nuclear charge of the ionizing agent (target) and z^* the effective charge of the projectile for binding the $1s$ electron (see Sec. IV B). The factor 2 accounts for the two $1s$ projectile electrons and N_A is the number of atoms in the target (2 for H_2 and 1 for He). $\sigma_{pH}(V_0/z^*)$ is the PWBA ionization cross section for $H^+ + H$ collisions (see Table III) computed as a function of scaled proton velocity V_0/z^* [86]. The $1s$ ionization potential of the Be-like ions, $i_{1s}(1s^22s^2)$, can be evaluated using

$$i_{1s} \equiv i_{1s}(1s^22s^2) = i_{2s}(1s^22s^2) + i_{2s}(1s^22s) + \varepsilon_A(^2S), \tag{20}$$

where $i_{2s}(1s^22s^2)$ and $i_{2s}(1s^22s)$ are the $2s$ ionization potentials for Be-like and Li-like configurations given in Ref. [87], while $\varepsilon_A(^2S)$ is the Auger electron energy of the

TABLE III. PWBA ionization cross sections [86], $\sigma_{pH}(V_0)$, for $p + H(1s) \rightarrow p + p + e^-$ vs proton velocity V_0. V_0 is in a.u., while σ_{pH} is in units of πa_0^2, where a_0 is the Bohr radius in a.u.

V_0	σ_{pH}[a]	V_0	σ_{pH}	V_0	σ_{pH}	V_0	σ_{pH}
0.05	4.28[−7]	0.2	0.0123	0.85	2.32	7	0.131
0.06	1.79[−6]	0.225	0.0255	0.9	2.38	8	0.1
0.07	5.97[−6]	0.25	0.0475	0.95	2.42	9	0.0786
0.08	1.67[−5]	0.275	0.0804	1	2.43	10	0.0629
0.09	4.12[−5]	0.3	0.127	1.25	2.27	12.5	0.0378
0.1	9.16[−5]	0.35	0.263	1.5	1.95	15	0.0239
0.11	1.87[−4]	0.4	0.475	1.75	1.63	17.5	0.0156
0.12	3.56[−4]	0.45	0.695	2	1.35	20	0.0103
0.13	6.38[−4]	0.5	0.958	2.5	0.935	22.5	0.00703
0.14	0.00109	0.55	1.23	3	0.673	25	0.00481
0.15	0.00177	0.6	1.49	3.5	0.505	27.5	0.00337
0.16	0.00278	0.65	1.72	4	0.39	30	0.00241
0.17	0.0042	0.7	1.92	5	0.256	32.5	0.00173
0.18	0.00616	0.75	2.09	6	0.179	35	0.00129
0.19	0.0088	0.8	2.22				

[a] Numbers in brackets imply multiplication by powers of 10.

^2S line given in Tables I and II. The values $i_{1s} = 665$ eV and $i_{1s} = 340$ eV were used for the O^{4+} and C^{2+} ($1s^22s^2$) ions, respectively. The cross section $\sigma_{enI}(E_p)$ obtained from Eq. (19) is plotted as a function of projectile energy E_p in Figs. 8, 9, and 2 as a dotted-dashed line.

B. Contributions from the electron-electron interaction

The e-e contribution to $1s$ ionization was calculated using the IA formulas Eqs. (6) and (8). In this case the $1s$ ionization cross section due to electron-electron interaction σ_{eeI} is related to the electron-impact $1s$ ionization cross section $\sigma_{eII}(1s, E_e)$ via Eq. (8),

$$\sigma_{eeI}(E_p) = \int \sigma_{eII}(1s, E_e) J(P_z') dP_z'. \quad (21)$$

Here $J(P_z')$ is the total Compton profile for the two equivalent electrons of the He or H_2 targets given in Ref. [52]. $\sigma_{eII}(1s, E_e)$ is given as [88]

$$\sigma_{eII}(1s, E_e) = \frac{n_{1s}}{z^{*4}} \sigma_R^{\mathrm{H}}(1s, u), \quad (22)$$

where z^* is the screened nuclear charge of the projectile for binding a $1s$ electron. For O^{4+}, $z^* = 8 - 0.65 = 7.35$, while for C^{2+}, $z^* = 6 - 0.65 = 5.35$ [88]. n_{1s} is the number of electrons in the projectile $1s$ shell and $\sigma_R^{\mathrm{H}}(1s, u)$ is the reduced eII cross section as calculated for a hydrogenic ion in the Coulomb-Born exchange approximation [88],

$$\sigma_R^{\mathrm{H}}(1s, u) = \frac{\pi a_0^2}{u} \left[1.13 \ln u + 4.41 \left(1 - \frac{1}{u}\right)^2 + \left(\frac{-2.00}{u} + \frac{3.80}{u^2}\right)\left(1 - \frac{1}{u}\right) \right], \quad (23)$$

where a_0 is the Bohr radius and u is the electron-impact energy in units of i_{1s}, i.e., $u = E_e/i_{1s}$.

The sum, $\sigma_K = \sigma_{enI} + \sigma_{eeI}$, is the PWBA-IA total K-shell ionization cross section. As seen in Figs. 8, 9, and 2 these calculations agree fairly well with the measured data.

V. DISCUSSION

Our interest in studying projectile ionization by electron spectroscopy grew out of our previous work on projectile excitation in which the presence of e-e interaction effects was found to be manifested by the sharp rise observed in the excitation cross section around the threshold for electron-impact excitation [7] [see also Fig. 10(a)]. The question arose as to whether the e-e interaction would also be manifested in the same way in projectile ionization and whether the IA could be successfully used to describe the energy dependence of the e-e contributions.

The present data, as well as the data of Ref. [8], do not offer a clear *qualitative* feature by which one can unambiguously identify eeI over the competing enI process. This is in contrast to the eeE process in which a clear threshold signals the presence of the e-e interactions. The much slower rise of σ_{eeI} is characteristic of the underlying electron-impact ionization process as shown in Fig. 10(b), and it reflects the infinity of continuum states available to ionization as opposed to the one discrete state available

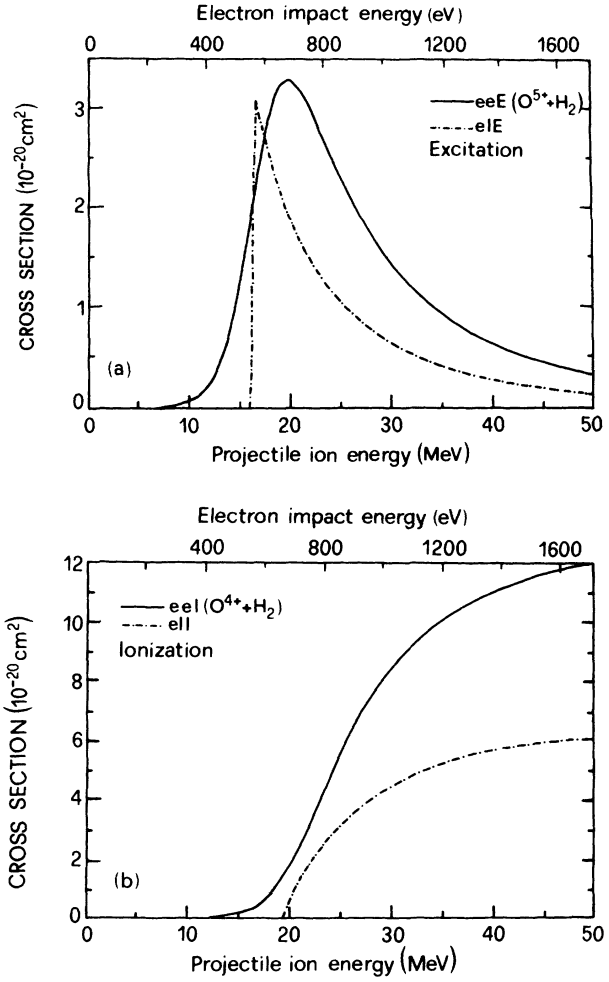

FIG. 10. (a) Excitation due to e-e interactions. Dashed line: Calculated $1s \rightarrow 2p$ electron-impact excitation (eIE) cross sections for the $1s2s2p\,^4P$ state production in $e^- + O^{5+}(1s^22s)$ collisions [7, 93] as a function of electron-impact energy (top scale). The eIE cross section is zero below the excitation threshold at $E_e = 562$ eV. Solid line: Calculated $1s \rightarrow 2p$ electron-electron excitation (eeE) cross section for the $1s2s2p\,^4P$ state production in $O^{5+}(1s^22s) + H_2$ collisions as a function of ion energy as computed by the IA formulation of Eq. (8) [7]. (b) Ionization due to e-e interactions. Dashed line: Calculated $1s$ electron-impact ionization (eII) cross section for $e^- + O^{4+}(1s^22s^2)$ collisions as a function of electron-impact energy (top scale) as computed from Eq. (22). The eII cross section is zero below the ionization threshold at $E_e = 664.6$ eV. Solid line: Calculated $1s$ electron-electron ionization (eeI) cross section for $O^{4+}(1s^22s^2) + H_2$ collisions as a function of ion energy as computed from Eq. (21). Both ion-atom collision cross sections assume two active electrons on the target. The sharpness of the electron-impact thresholds for excitation and ionization is seen to be quite different. The energy scale on the top of the figure refers to an electron of impact energy E_e (eV) which has the same velocity as an ion of energy E_p (MeV).

for excitation in the electron-impact excitation process [93] underlying eeE as seen in Fig. 10(a).

The absence of a sharp threshold for the onset of ionization is quite evident in the case of O^{4+} projectiles, where all the ionization data seen in Fig. 8 can also be fitted by just the enI calculation *alone* with an appropriate rescaling. Hence, the claim that eeI has been experimentally observed with these data rests to a large extent on the faith we have in our enI and eeI calculations. More data points at energies well above the ionization threshold need be obtained for O^{4+} for an improved test of electron-electron interaction effects. In contrast, for the case of C^{5+} and C^{2+} projectiles, as seen in Figs. 2 and 9, a rescaling of the enI calculation alone will not fit the data; the eeI contributions are clearly necessary.

Also included for comparison in Figs. 8 and 9 are the results of the screening-antiscreening calculation in a coherent treatment of enI and eeI [90]. An incoherent treatment (not shown) gives very similar results. The agreement between the screening-antiscreening and the PWBA-IA calculations is rather good. This good agreement is also demonstrated in Fig. 2, in which our PWBA-IA ionization calculations for $C^{5+} + H_2$ are compared to the experimental data of Hülskötter *et al.* [8] and their screening-antiscreening calculations. Thus, both screening-antiscreening and PWBA-IA calculations give very similar results in the case of ionization. However, the screening-antiscreening model, while providing a good description of the ionization cross sections well above threshold, includes the electron-impact cross sections in a rather unsatisfying *ad hoc* formulation [90, 9]. This gives rise to an artificially sharp threshold behavior for ionization which can be eliminated to first order with a more elaborate treatment of the closure approximation [90] required in the evaluation of the screened target charge $Z^*(q)$ [see Eq. (2)]. In contrast, the IA formulation is seen to give a good account of the threshold behavior of both ionization, as discussed in this article, and excitation [7]. This is not surprising, since the threshold behavior is built into the model from the beginning. Since threshold effects are much sharper in $1s$ excitation data [7, 12], the region around the excitation threshold might provide a more sensitive testing ground for investigating any observable differences between the IA and the screening-antiscreening approaches.

Two basic assumptions have been adopted in the data analysis of the present K-shell ionization study: isotropic Auger electron emission and needle ionization. Under these assumptions, a means of determining the metastable fraction of the beam was developed which was essential for the final determination of the K-shell ionization cross sections.

The validity of isotropy depends on the nonalignment of the states produced in the collision. If the excitation and ionization states formed in the collision were aligned, then the Auger electron angular distributions would be nonisotropic. In that case, the determination of the metastable fraction according to Eqs. (15) or (17) would not be correct, and the resulting ionization cross sections would also be incorrect. The fact that the metastable beam fractions computed by both methods, i.e., Eqs. (15) and (17), agree, argues in favor of nonalignment. This is also supported by the observed agreement between our measured ionization cross sections and those computed by theory. We note that the final ionization cross section was computed according to Eq. (18) using only the ^2S electron yields, known from theory to be isotropic, to minimize any effects due to alignment.

The validity of needle ionization is based on x-ray [35, 61] and Auger [53, 78, 79] spectroscopic studies. In collisions with low-Z targets, the projectile-electron spectra are quite simple with just a few lines, indicating the existence of states resulting primarily from single-electron processes, i.e., either single-electron excitation or single-electron ionization. This is in contrast to collisions with high-Z targets (e.g., Ar), in which much more complicated line spectra are obtained, indicating the existence of a variety of multielectron processes resulting in many different projectile charge states [93, 78]. In particular, for our Be-like projectiles, most of the observed lines (see Figs. 3 and 4) have been assigned [56] to the decay of Li-like and Be-like states which result from direct $1s$ ionization or $1s \rightarrow 2p$ excitation. Certainly, if double-excitation mechanisms were substantial, needle-ionization conditions would not prevail. For example, the double-excitation process of $1s \rightarrow 2p$ excitation accompanied by $2s$ ionization would lead to the production of the ^4P, $^2P_-$, and $^2P_+$ states from the $1s^2 2s^2\ ^2S$ ground state rather than from the $1s^2 2s 2p\ ^3P$ metastable state as assumed in this analysis. That this two-electron process does not occur in collision in the energy range of our ionization studies is indicated by x-ray spectroscopic studies [94] of satellite and hypersatellite lines of 15-MeV F^{q+} + He.

We also note that in the PWBA calculation of σ_{enI} using Eq. (19), we have assumed that the molecular hydrogen target is equivalent to two atomic hydrogen targets. This assumption, while still not experimentally tested, seems to be theoretically valid for the ionization of projectiles with $Z_p \geq 5$ [10]. It would be of interest to check this experimentally using an atomic hydrogen target.

Prior experimental studies of eeI have used the more traditional charge analysis technique [8–10]. It is therefore of interest to discuss the limitations of the two methods. The Auger-spectroscopy method must use projectiles having at least three electrons initially (two of which must not be in the K shell) and requires the validity of isotropy and needle-ionization conditions for the final determination of total ionization cross sections. The charge-analysis method used in Refs. [8–10], while directly providing ionization cross sections of H-like projectiles, cannot be applied to the study of K-shell ionization of many-electron projectiles, since, apart from the obvious complications due to contributions from shells higher than the K shell, the process of excitation followed by autoionization cannot be readily separated from the direct K-shell ionization channel. This is particularly true for light ions, where excitation autoionization can be substantial [79], as demonstrated by the existence of excitation lines in our spectra contributing up to 30% of the

total K-vacancy production cross section. It would thus seem appropriate to use both experimental methods to span the full range of available charge states and provide a more complete test of theory.

VI. CONCLUSIONS

In this study we have applied 0° Auger-spectroscopy techniques to measure projectile $1s$ ionization cross sections in energetic collisions of Be-like C^{2+} and O^{4+} projectiles with H_2 and He targets. In contrast to our experience with the electron-electron interaction in projectile excitation, where relatively sharp thresholds were observed, no such thresholds effects were observable in ionization.

However, as in the case of excitation, we found that the impulse approximation (IA) could provide a simple formula for calculating the contributions of electron-electron interactions to ionization. Combined with a PWBA calculation of electron-nucleus interaction contributions, the calculation agreed well with the experimental total ionization cross sections. Calculations using the screening-antiscreening approach based on the Born approximation were also performed and found to be in good agreement with both our data and the PWBA-IA calculations.

The Auger-spectroscopy cross sections for $1s$ ionization of Be-like ions were found to be very similar to those reported for H-like ions which used the charge analysis method to identify the ionization channel. The Auger-spectroscopy method extends the possible range of ionization studies to ions with more than three electrons, since for these ions charge analysis cannot be readily used to distinguish K-shell ionization.

Finally, we note that we have also determined the fraction of the beam in the metastable $1s^2 2s 2p\ ^3P$ state, using measured Auger electron yields and fractional-parentage coefficients. The metastable beam fraction was found to be large, close to 61% for the O^{4+} projectiles.

The good agreement between K-shell ionization data and the PWBA-IA calculations indicates the success of the IA in describing the contribution of the electron-electron interaction in ionization for the systems investigated. This study practically completes the list of ion-atom processes to which the IA has been successfully applied, which includes radiative electron capture (REC), resonance transfer excitation (RTE), electron-electron excitation (eeE), binary encounter electron (BEe) production, and now electron-electron ionization (eeI). Indeed, the IA has provided us with a remarkably simple intuitive picture of electron-electron interactions in ion-atom collisions. Future studies of electron-electron interactions can explore the limits of the applicability of the IA picture by investigating slower collisions, as well as collisions with atomic hydrogen and Rydberg atoms.

ACKNOWLEDGMENTS

We gratefully acknowledge discussions with C.P. Bhalla, C.D. Lin, W.E. Meyerhof, and N. Stolterfoht. This work was supported by the Division of Chemical Sciences, Office of Basic Energy Sciences, Office of Energy Research, U.S. Department of Energy. One of us (T.J.M.Z.), would like to acknowledge the support of NATO collaborative research Grant No. CRG-910567.

---

* Present address: Brookhaven National Laboratory, Department of Applied Science, Upton, NY 11973.

† Present address: Physics Department, University of Crete and Institute of Electronic Structure & Laser, P.O. Box 1527, Heraklion 711 10, Crete, Greece.

[1] J.H. McGuire, N. Stolterfoht, and P.R. Simony, Phys. Rev. A **24**, 97 (1981).

[2] U. Thumm, J.S. Briggs, and O. Schöller, J. Phys. B **21**, 833 (1988).

[3] R.D. Dubois and L.H. Toburen, Phys. Rev. A **38**, 3960 (1988).

[4] R. Anholt, W.E. Meyerhof, H. Gould, Ch. Munger, J. Alonso, P. Thieberger, and H.E. Wegner, Phys. Rev. A **32**, 3302 (1985).

[5] R. Hippler, S. Datz, P.D. Miller, P.L. Pepmiller, and P.F. Dittner, Phys. Rev. A **35**, 585 (1987).

[6] T.N. Tipping, J.M. Sanders, J. Hall, J.L. Shinpaugh, D.H. Lee, J.H. McGuire, and P. Richard, Phys. Rev. A **37**, 2906 (1988).

[7] T.J.M. Zouros, D.H. Lee, and P. Richard, Phys. Rev. Lett. **62**, 2261 (1989).

[8] H.-P. Hülskötter, W.E. Meyerhof, E. Dillard, and N. Guardala, Phys. Rev. Lett. **63**, 1938 (1990).

[9] H.-P. Hülskötter, B. Feinberg, W.E. Meyerhof, A. Belkacem, J.R. Alonso, L. Blumenfeld, E.A. Dillard, H. Gould, N. Guardala, G.F. Krebs, M.A. McMahan, M.E. Rhoades-Brown, B.S. Rude, J. Schweppe, D.W. Spooner, K. Street, P. Thieberger, and H.E. Wegner, Phys. Rev. A **44**, 1712 (1991).

[10] W.E. Meyerhof, H.-P. Hülskötter, Qiang Dai, J.H. McGuire, and Y.D. Wang, Phys. Rev. A **43**, 5907 (1991).

[11] P. Richard, in *X-Ray and Inner-Shell Processes*, edited by T.A. Carlson, M.O. Krause, and S.T. Manson, AIP Conf. Proc. No. 215 (AIP, New York, 1990), pp. 315–334.

[12] D.H. Lee, T.J.M. Zouros, J.M. Sanders, and P. Richard (unpublished).

[13] P. Richard, D.H. Lee, T.J.M. Zouros, J.M. Sanders, and J.L. Shinpaugh, J. Phys. B **23**, L213 (1990).

[14] T.J.M. Zouros, P. Richard, and D.H. Lee, in *Proceedings of the 4th Workshop on High-Energy Ion-Atom Collisions Processes, Debrecen, Hungary, 1990*, edited by D. Berényi and G. Hock (Springer-Verlag, Berlin, 1991).

[15] C. Kelbch, S. Hagmann, S. Kelbch, R. Mann, R.E. Olson, S. Schmidt, and H. Schmidt-Böcking, Phys. Lett. A **139**, 304 (1989).

[16] C. Kelbch, R.E. Olson, S. Schmidt, S. Hagmann, and H. Schmidt-Böcking, J. Phys. B **22**, 2171 (1989).

[17] C.O. Reinhold, D.R. Schultz, and R.E. Olson, J. Phys. B **23**, L591 (1990).

[18] R. Shingal, Z. Chen, K.R. Karim, C.D. Lin, and C.P. Bhalla, J. Phys. B **23**, L637 (1990).

[19] K. Taulbjerg, J. Phys. B **23**, L761 (1990); **24**, 2529

(1991).
[20] C.O. Reinhold, D.R. Schultz, R.E. Olson, C. Kelbch, R. Koch, and H. Schmidt-Böcking, Phys. Rev. Lett. **66**, 1842 (1991).
[21] T.B. Quinteros, A.D. Gonzalez, O. Jagutzki, A. Skutlartz, D.H. Lee, S. Hagmann, P. Richard, C. Kelbch, S.L. Varghese, and H. Schmidt-Böcking, J. Phys. B **24**, 1377 (1991).
[22] T. Quinteros and J.F. Reading, Nucl. Instrum. Methods Phys. Res. Sect. B **53**, 363 (1991).
[23] O. Jagutzki, S. Hagmann, H. Schmidt-Böcking, R.E. Olson, D.R. Schultz, R. Dörner, R. Koch, A. Skutlartz, A. Gonzalez, T.B. Quinteros, C. Kelbch, and P. Richard, J. Phys. B **24**, 2579 (1991).
[24] E. Merzbacher and H.W. Lewis, in *Corpuscles and Radiation,* edited by F. Flügge, Vol. 34 of *Encyclopedia of Physics* (Springer, Berlin 1958).
[25] D.H. Madison and E. Merzbacher, in *Atomic Inner Shell Processes,* edited by B. Crasemann (Academic, New York, 1975), Chap. 1.
[26] J.M. Hansteen, in *Advances in Atomic and Molecular Physics II,* edited by D.R. Bates and B. Bederson (Academic, New York, 1975), Vol. II, p. 299.
[27] S.T. Manson, L.H. Toburen, D.H. Madison, and N. Stolterfoht, Phys. Rev. A **12**, 60 (1975).
[28] G. Basbas, W. Brandt, and R. Laubert, Phys. Rev. A **17**, 1655 (1978).
[29] G.H. Gillespie, Phys. Rev. A **18**, 1967 (1978).
[30] D.H. Lee, P. Richard, T.J.M. Zouros, J.M. Sanders, J.L. Shinpaugh, and H. Hidmi, Phys. Rev. A **41**, 4816 (1990).
[31] D.R. Bates and G.W. Griffing, Proc. Phys. Soc. London Sect. A **66**, 961 (1953); **67**, 663 (1954); **68**, 90 (1955).
[32] J.S. Briggs and K. Taulbjerg, in *Topics in Current Physics,* edited by I. Sellin (Springer, New York, 1978), Vol. 5, p.106.
[33] N. Stolterfoht, in *Topics in Current Physics,* edited by I. Sellin (Springer, New York, 1978), Vol. 5, p.155.
[34] L.H. Toburen and W.E. Wilson, Radiat. Res. **82**, 29 (1979).
[35] H. Tawara, M. Terasawa, P. Richard, T.J. Gray, P. Pepmiller, J. Hall, and J. Newcomb, Phys. Rev. A **20**, 2340 (1979).
[36] S.T. Manson and L.H. Toburen, Phys. Rev. Lett. **46**, 529 (1981).
[37] L.H. Toburen, N. Stolterfoht, P. Ziem, and D. Schneider, Phys. Rev. A **24**, 1741 1981).
[38] R. Anholt, Phys. Lett. **114A**, 126 (1986).
[39] P. Eisenberger and P.M. Platzman, Phys. Rev. A **2**, 415 (1970).
[40] M. Kleber and D.H. Jakubassa, Nucl. Phys. **A252**, 152 (1975).
[41] J.S. Briggs, J. Phys. B **10**, 3075 (1977).
[42] D. Brandt, Phys. Rev. A **27**, 1314 (1983); J.M. Feagin, J.S. Briggs, and T.M. Reeŭes, J. Phys. B **17**, 1057 (1984).
[43] RTE is a correlated two-electron process, involving the excitation of a projectile electron with the simultaneous transfer of a target electron to the projectile, resulting from the direct *e-e* interaction between the transferred (target) and excited (projectile) electrons. For recent reviews see J.A. Tanis, Nucl. Instrum. Methods Phys. Res. Sect. B **40/41**, 70 (1989); Y. Hahn and K.J. La Gattuta, Phys. Rep. **166**, 195 (1988) and references therein.
[44] J.H. McGuire, Adv. Atm. Mol. Opt. Phys. **29**, 217 (1992); N. Stolterfoht, in *Electron Correlation Processes in Energetic Ion-Atom Collisions,* edited by V. Florescu and V. Zoran (World Scientific, Singapore, 1989); J.H. McGuire, Phys. Rev. A **36**, 1114 (1987); R.L. Becker, A.L. Ford, and J.F. Reading, *ibid.* **29**, 3111 (1984).
[45] M.L. Goldberger and K.M. Watson, *Collision Theory* (Krieger, Huntington, NY, 1975), p. 683.
[46] J.K. Swenson, Y. Yamazaki, P.D. Miller, H.F. Krause, P.F. Dittner, P.L. Pepmiller, S. Datz, and N. Stolterfoht, Phys. Rev. Lett. **57**, 3042 (1986).
[47] Y. Hahn, Phys. Lett. A**119**, 293 (1986).
[48] Y. Hahn, Commun. At. Mol. Phys. **19**, 99 (1987).
[49] M. Schulz, J.P. Giese, J.K. Swenson, S. Datz, P.F. Dittner, H.F. Krause, H. Schöne, C.R. Vane, M. Benhenni, and S.M. Shafroth, Phys. Rev. Lett. **62**, 1738 (1989).
[50] Y. Hahn and H. Ramadan, Phys. Rev. A **40**, 6206 (1989).
[51] D.H. Lee, Ph.D. dissertation, Kansas State University, 1990.
[52] J.S. Lee, J. Chem. Phys. **66**, 4906 (1977); F. Biggs, L.B. Mendelsohn, and J.B. Mann, At. Data Nucl. Data Tables **16**, 201 (1975).
[53] A. Itoh, T. Schneider, G. Schiwietz, Z. Roller, H. Platten, G. Nolte, D. Schneider, and N. Stolterfoht, Phys. B **16**, 3965 (1983).
[54] N. Stolterfoht, Phys. Rep. **146**, 315 (1987).
[55] The lifetime τ of the $1s^2 2s 2p\,^3P$ metastable state for C^{2+} and O^{4+} is very long. The $J = 2$ substate decays via $M2$ transitions with $\tau_{J=2} = 47$ s and 199 s for O^{4+} and C^{2+}, respectively [see P. Shorer and C.D. Lin, Phys. Rev. A **16**, 2068 (1977)]. The $J = 1$ substate decays by spin-forbidden dipole transitions with a radiative lifetime $\tau_{J=1} = 4.3 \times 10^{-4}$ s and 9.5×10^{-3} s for O^{4+} and C^{2+}, respectively [see C.D. Lin and W.R. Johnson, Phys. Rev. A **15**, 1046 (1977)]. Finally, the $J = 0$ substate decays via a two-photon ($E1 + M1$) transition with a lifetime $\tau_{J=0} > \tau_{J=2}$ [C.D. Lin (private communication)].
[56] R. Bruch, N. Stolterfoht, S. Datz, P.D. Miller, P.L. Pepmiller, Y. Yamazaki, H.F. Krause, and J.K. Swenson, Phys. Rev. A **35**, 4114 (1987).
[57] D.H. Lee, T.J.M. Zouros, J.M. Sanders, J.L. Shinpaugh, T.N. Tipping, S.L. Varghese, B.D. DePaola, and P. Richard, Nucl. Instrum. Methods Phys. Res. Sect. B **40/41**, 1229 (1989).
[58] N. Stolterfoht, D. Schneider, R. Burch, H. Wieman, and J.S. Risley, Phys. Rev. Lett. **33**, 59 (1974).
[59] J.E. Miraglia and J. Macek, Phys. Rev. A **43**, 5919 (1991).
[60] D.H. Lee, P. Richard, J.M. Sanders, T.J.M. Zouros, J.L. Shinpaugh, and S.L. Varghese, Nucl. Instrum. Methods Phys. Res. Sect. B **56/57**, 99 (1991).
[61] M. Terasawa, T.J. Gray, S. Hagmann, J. Hall, J. Newcomb, P. Pepmiller, and P. Richard, Phys. Rev. A **27**, 2868 (1983).
[62] An independent quantum-mechanical impulse-approximation calculation [59] has shown that the IA treatment described here, when applied to BE*e* production in collisions of bare ions with H_2, is good only for projectiles with $Z_p \leq 15$. An independent check on our absolute normalization was also provided by recent measurements of $2p$ electron-capture cross sections in $F^{7+} + H_2$ (or He) collisions using Auger-electron spectroscopy [60]. Good agreement was found with previous high-resolution x-ray measurements [61].

[63] K.R. Karim and C.P. Bhalla (private communications).
[64] B.F. Davis and K.T. Chung, Phys. Rev. A **39** 3942 (1989).
[65] B.F. Davis and K.T. Chung, Phys. Rev. A **36**, 1948 (1987).
[66] M.H. Chen and B. Crasemann, Phys. Rev. A **27**, 544 (1983).
[67] R. Mann, Phys. Rev. A **35**, 4988 (1987).
[68] R. Bruch, K.T. Chung, W.L. Luken, and J.C. Culberson, Phys. Rev. A **31**, 310 (1985).
[69] D. Schneider, R. Bruch, W.H.E. Schwarz, T.C. Chang, and C.F. Moore, Phys. Rev. A **15**, 926 (1977).
[70] M. Rødbro, R. Bruch, and P. Bisgaard, J. Phys. B **12**, 2413 (1979).
[71] E. Høloien and S. Geltman, Phys. Rev. **153**, 81 (1967).
[72] M.H. Chen, At. Nucl. Data Tables **34**, 301 (1986).
[73] U.I. Safronova and V.N. Kharitonova, Opt. Spektrosk. **27**, 550 (1969) [Opt. Spectrosc. **27**, 300 (1969)].
[74] K.T. Chung, Phys. Rev. A **42**, 645 (1990).
[75] E. Träbert, Nucl. Instrum. Methods B **23**, 287 (1987).
[76] D. Charalambidis, R. Brenn, and K.J. Koulen, Phys. Rev. A **40**, 2359 (1989).
[77] Lifetime effects on the detection of Auger electrons from the long-lived ^4P state were accounted for in an effective solid-angle correction. It was found that the detection efficiency of the ^4P Auger electrons produced between the exit of the gas cell assembly and the spectrometer entrance is larger than for electrons produced inside the gas cell. These corrections are included in the factor G_Ω described in detail in Ref. [51]. F_m is then given from Eqs. (15), (13), and (14) in terms of single differential Auger-electron yields $dY_L/d\Omega$ measured at 0° as

$$F_m = \left[1 + \frac{\frac{1}{\xi_{2S}}\frac{dY_{2S}}{d\Omega}}{\frac{G_\Omega}{\xi_{4P}}\frac{dY_{4P}}{d\Omega} + \frac{1}{\xi_{2P_-}}\frac{dY_{2P_-}}{d\Omega} + \frac{1}{\xi_{2P_+}}\frac{dY_{2P_+}}{d\Omega}}\right]^{-1},$$

where isotropic emission of Auger electrons has been assumed. A study of G_Ω showed this factor to vary between 0.35 and 0.57, depending on projectile energy and target species, resulting in an overall variation of F_m between 0.56 and 0.63. G_Ω was also experimentally determined to be about 0.5 for ^4P states produced in 4.75- and 19-MeV O^{5+} + He collisions. The details of this measurement are described in Refs. [12] and [51].
[78] A. Itoh, D. Schneider, T. Schneider, T.J.M. Zouros, G. Nolte, G. Schiwietz, W. Zeitz, and N. Stolterfoht, Phys. Rev. A **31**, 684 (1985).
[79] N. Stolterfoht, P.D. Miller, H.F. Krause, Y. Yamazaki, J.K. Swenson, R. Bruch, P.F. Dittner, P.L. Pepmiller, and S. Datz, Nucl. Instrum. Methods Phys. Res. Sect. B **24/25**, 168 (1987).
[80] C.D.H. Chisholm, A. Dalgarno, and F.R. Innes, in *Advances in Atomic and Molecular Physics*, edited by D.R. Bates and I. Estermann (Academic, New York, 1969), Vol. 5, pp. 297–335.
[81] Ionization of a 1s electron of the metastable state can contribute to the formation of *either* $^2P_-$ and $^2P_+$ *or* the ^4P state. Hence, the probability of producing the ^4P state is the same as the sum of the probabilities for producing the $^2P_-$ and $^2P_+$ states.
[82] J.M. Anthony (unpublished); Anthony computed the metastable beam fraction for C^{2+} beams using Eq. (17), but neglecting the contamination from the $1s2s^22p\,^3P$ state which was assumed negligible. Using the C^{2+} + H_2 electron yields measured here (see Fig. 4) and also assuming the contribution of the $1s2s^22p\,^3P$ state to be small (see Fig. 6), an average value of $F_m = 0.63$ for C^{2+} beams was obtained using Eq.(17).
[83] B. Cleff and W. Mehlhorn, J. Phys. B **7**, 593 (1974).
[84] J. Eichler and W. Fritsch, J. Phys. B **9**, 1477 (1976).
[85] W. Mehlhorn (unpublished), p. 107.
[86] D.R. Dillingham, M.S. thesis, Kansas State University, 1980.
[87] C.E. Moore, *Atomic Energy Levels*, Natl. Bur. Stand. Ref. Data Ser., Natl. Bur. Stand. (U.S.) Circ. No. 35 (U.S. GPO, Washington, D.C., 1971), Vol. 1.
[88] D.L. Moores, L.B. Golden, and D.H. Sampson, J. Phys. B **13**, 385 (1980).
[89] S.J. Goett and D.H. Sampson, At. Data Nucl. Data Tables **29**, 535 (1983).
[90] These calculations involved the evaluation of the cross section appearing in Eq. (1). For the projectiles, hydrogenic wave functions were used with an effective 1s binding energy of 340 and 665 eV for C^{2+} and O^{4+} ions, respectively. The computed K shell ionization cross sections were multiplied by 2 to account for two electrons in the K shell of the projectile. Finally, for the integration over momentum transfer q [see Eqs. (1) and (2)], an upper limit on q of less than 150 a.u. was used in calculating all e-n cross sections, while true maximum projectile-electron-momentum transfers were used in calculating all e-e cross sections. For the integration over ejected electron energies ϵ [see Eq. (1)], an upper limit of 50 a.u. was used in all cases. For the targets, hydrogenic wave functions were also assumed with $Z = 2$ and 1 for He and H_2, respectively [see Eq. (2)]. Molecular effects were assumed to be negligible in the total cross-section calculations for the H_2 target as shown in Refs. [10] and [91]. A value of Z=1.76 was also tried for He, but the results did not change appreciably.
[91] Y.D. Wang and J.H. McGuire, Nucl. Instrum. Methods Phys. Res. Sect. B **56/57**, 300 (1991).
[92] E.C. Montenegro and W.E. Meyerhof, Phys. Rev. A **43**, 2289 (1991).
[93] D. Schneider, C.F. Moore, and B.M. Johnson, J. Phys. B **9**, L153 (1976).
[94] H. Tawara, P. Richard, K.A. Jamison, T.J. Gray, J. Newcomb, and C. Schmiedekamp, Phys. Rev. A **19**, 1960 (1979).